Chemical Engineering & Processing: Process Intensification 117 (2017) 186–194

Contents lists available at ScienceDirect

Chemical Engineering & Processing: Process Intensification

journal homepage: www.elsevier.com/locate/cep

Analysis of focused indirect ultrasound via high-speed spatially localized pressure sensing and its consequences on nucleation

Mo Jiang, Chen Gu, Richard D. Braatz*

Massachusetts Institute of Technology,77 Massachusetts Avenue, Cambridge, MA, 02139, USA

ARTICLE INFO

Keywords:
Process intensification
Ultrasonication
Nucleation
Tubular crystallization
Pinducer
Process design

ABSTRACT

Ultrasonication is frequently used to promote crystallization and chemical reactions, with many papers reporting the effects of ultrasonic parameters. High-speed pressure inducers (aka pinducers) and signal processing are used here to gain insights into the spatial localization of energy dissipation that occurs during ultrasonication, facilitating a design that allows ultrasonication to be spatially localized inside a tube, without requiring that the probe directly contact the solution. The fluid pressure measured inside of a flexible silicone tube pressed against an ultrasonic probe is observed to move between nearly constant amplitude oscillations to variable shape and amplitude waveforms that deviate significantly from being periodic. Ultrasonic power is transferred to the fluid inside the tube, generating a wide frequency range including via bubble oscillations. Discrete Fourier Transform analysis indicates complex interactions within the experimental system, in addition to the energy transferred inside the tubing at the expected ultrasonic source frequency. The total acoustic intensity decays exponentially with distance from the zone, dropping by more than two orders-of-magnitude for each 1 cm increase in distance. The pinducer data analyses guide the design of an experimental setup in which crystals nucleate within fluid inside the zone in the tube, right under the ultrasonic probe.

1. Introduction

Ultrasonication has been widely used in daily life and research laboratories, such as glass surface cleaning, pigment dispersion, metal casting, cell disruption, and facilitation of crystallizations and chemical/polymeric reactions [1–13], related to the phenomenon of acoustic cavitation (growth and collapse of microbubbles under an ultrasonic field) [1,14–16]. Ultrasonication has also been used to aid crystallization, such as accelerating nucleation, reducing crystal size, reducing aggregation, or changing polymorphic ratios [4,8–11,13]. Although the exact sonocrystallization mechanism remains to be established [4,15,17,18], several ultrasonic parameters (e.g., ultrasonic intensity or power, time, and volume [1,4,5,19]) have been identified effective in enhancing the control of crystallization processes.

Most bench-scale continuous sonocrystallization researches are based on configurations including an ultrasonic probe or bath. The advantages of probes (most directly inserted into/towards the solution as in Refs. [11–13,20,21]) include that (1) an ultrasonic probe can deliver much higher ultrasound intensity than the ultrasonic bath, with convenient adjustment of power [11–13,20,21]; and (2) there are usually more options of commercially available probes with different shapes and sizes [22]. Ultrasonic baths (where the container was placed such as in Refs. [17,23]) also have advantages, such as (1) lower requirement on sample thermal stability and temperature control, with less contamination probability due to no direct contact with solution; and (2) flexible container shape [17]. A recent multiphase millifluidic tubular crystallizer design combined the advantage of probe (focused energy) and bath (indirect ultrasonication) for its continuous nucleation process, tuning nuclei size with the ultrasonic amplitude [5].

With existing studies as a good starting point, the below questions remain to be answered for future ultrasonication-based nucleation designs: (1) how to narrow the nuclei size distribution, which directly affects the size distribution of product crystals [5,17,24]; (2) how to increase the scalability of the ultrasonication process without having to acquire new equipment [14,25]; and (3) will the ultrasound intensity remain the same if running continuously instead of as short pulses [26]. These questions cannot be addressed easily during crystallizations, which would require many trial-and-error experiments, costing time and materials.

To efficiently approach the above questions and better understand the process, this article measures and analyzes the “primary effect” (this term is used as in Ref. [14]) of ultrasonication, which can directly affect the commonly studied crystallization outcome (the “secondary effect”). The pressure is chosen for measurement, as the direct consequence of

* Corresponding author.
E-mail address: braatz@mit.edu (R.D. Braatz).

http://dx.doi.org/10.1016/j.cep.2017.04.008
Received 23 August 2016; Received in revised form 27 January 2017; Accepted 18 April 2017
Available online 22 April 2017

ultrasonication into liquid is a pressure wave, which causes while being affected by other phenomena such as the generation of micro-bubbles (cavities) and high temperature [4]. Hydrophones are sensors that measure liquid pressures based on a piezoelectric transducer that generates electricity when subjected to a pressure change (e.g., at pulse-mode ultrasonication [6,14]). This article employs a pinducer [6,27], which is a hydrophone of small geometric size (to minimize possible effects on the acoustic field), to measure pressures at multiple spatial locations during continuous ultrasonication.

This article is the first to use a pinducer to facilitate the design and optimization of a crystallization process, specifically, a nucleation subsystem based on a focused indirect ultrasonication zone to enhance reproducibility and the control of nuclei size distribution. Compared to most past ultrasound-aided crystallization studies that focused on the effect and final outcome of the ultrasonication generator's parameters (e.g., power input, frequency) or additive conditions on crystallization [1–4,10,12,13], we quantify the direct pressure consequence of ultrasonication at different configurations for guiding the nucleation process design, which adds value to past studies. With intensified learning of physical phenomena (e.g., bubble dynamics) based on the straightforward signal data analysis (not a "black-box"), this article also provides deeper insights and optimization suggestions for ultrasonication-involved crystallization designs, using tubular nucleation as an example (e.g., with more localized ultrasonic region than in [5]).

2. Materials and methods

2.1. Sonication and pinducer equipment

The experimental setup for pinducer measurement (Fig. 1) consists of an ultrasonic processor (Sonics® VCX750, frequency 20 kHz, input electric power 750 W), an ultrasonic probe (Sonics® 25 mm solid full wave probe, made of Titanium alloy Ti-6Al–4 V) to induce mechanical vibrations, a pressure transducer (pinducer) as a signal receiver (Belden 8216 RG-174/U Type 1C26), and a tube (Masterflex BioPharm Plus platinum-cured silicone tubing, ~3 mm inner diameter, ~6 mm outer diameter) connected front-to-end and filled with deionized water, all inside a plastic tray container of water. The ultrasonic processor and probe, and silicone tube used for pinducer measurement were the same models/operation conditions (e.g., ultrasonic amplitude at 50% of max amplitude) as in a recent continuous crystallizer design with ultrasound-aided nucleation [5]. In this article, only relatively low-frequency ultrasonication (20 kHz) is used, in comparison to high-frequency ultrasonication used for attenuation spectroscopy (e.g., 1–150 MHz as in Ref. [28]).

A needle-shaped pinducer with a tip diameter of 0.28 cm was inserted into the tubing (with the tip inside the fluid inside the tubing) to measure the pressure voltage inside the tubing without significantly changing the tubing geometry. The measurement part of pinducer is its tip only (according to the vendor). The signal from pinducer is sent to a data acquisition board (NI PXI-5105 12-bit 60 MS/s digitizer) installed in a personal computer running Microsoft Windows running LabVIEW, version 2011 that stores time-stamped data onto a hard drive. The data acquisition setup and operator is the same for rock physics [27], except that neither physical amplifier nor filter was used, based on the signal strength. After a warmup time of 1 min (with ultrasonication on), a total number of 82 continuous time signals of pressure voltage (referred to as "traces" [27], in unit of voltage, see Fig. 2 for examples) were collected within 5 min of continuous ultrasonication, meaning an interval of ~3.7 s. For each trace, the first 0.1 s was recorded without reducing the speed of collection (these data rates fill the computer's random access memory, with the data saved to a disk drive after each experiment). The temperature of water inside the plastic tray container was measured and confirmed to show no evident heating before and after the continuous ultrasonication. After the experiments, the data were analyzed and plotted (e.g., Figs. 2–4) using Matlab (version 2013b).

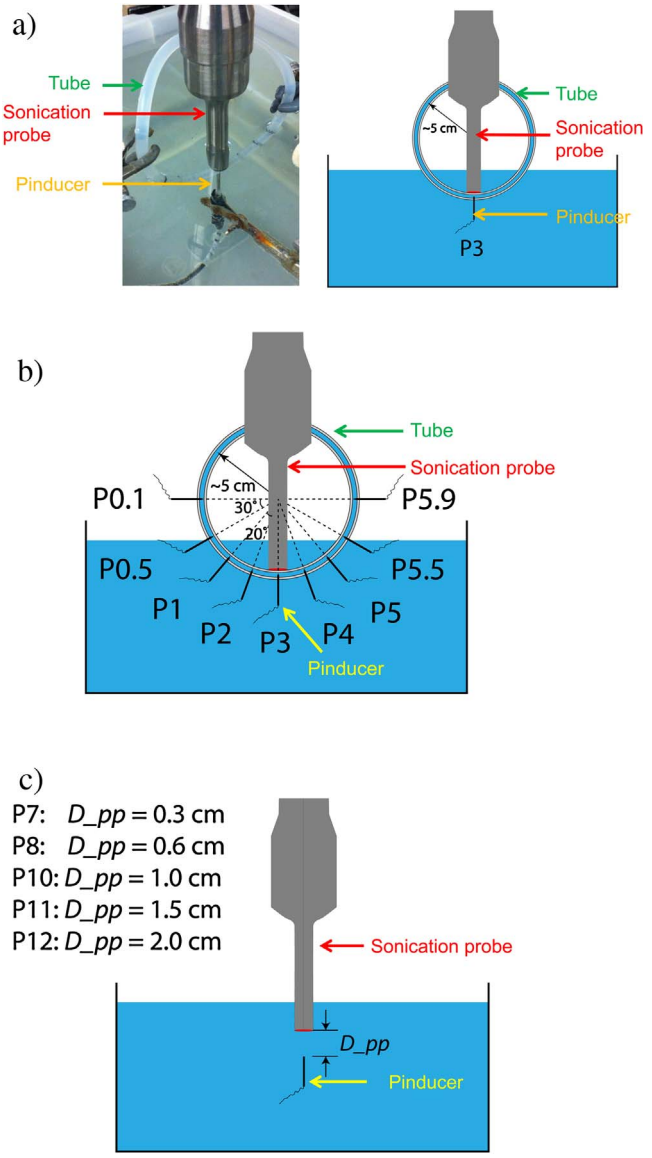

Fig. 1. (a) (Left) Photograph and (right) diagram of one measurement location (P3 in Fig. 1b) of the pinducer setup for pressure measurement inside the tubing. The ultrasonic probe was pressed against the outer wall of tubing, to which the pinducer was inserted perpendicularly. (b) Diagrams of various measurement locations (P0.1, P0.5, P1, P2, P3, P4, P5, P5.5, P5.9) of the pinducer setup for pressure measurement inside the tubing. The pinducer was inserted into the tube at different distances (1/18 or 1/12 of a circle of ~5 cm diameter between adjacent measurement points as labelled 20° or 30°, respectively) from the ultrasonic probe (e.g., "P3" whose photo is Fig. 1a). (c) Diagrams of various measurement locations (P7, P8, P10, P11, P12) of the pinducer setup for pressure measurement along the centerline of the ultrasonic probe (*D_pp* is the distance from measurement location to probe top along the centerline). No tubing was used in (c). For (a) to (c), experimental details are described in Subsection 2.1 and Table 1.

2.2. Nucleation validation and materials

Based on the learnings from the pinducer experiments described above, an ultrasound-aided cooling nucleation validation experiment was designed, with detailed justification in Subsection 3.2. The nucleation setup (configuration in Fig. 5) used the same ultrasonic equipment and conditions (e.g., focused indirect ultrasonic configuration, ultrasonic amplitude, media choice of water, and tubing choice) as for the pinducer measurement. The nucleation occurs inside of a solution of fluid inside of the tube. L-asparagine monohydrate (purity

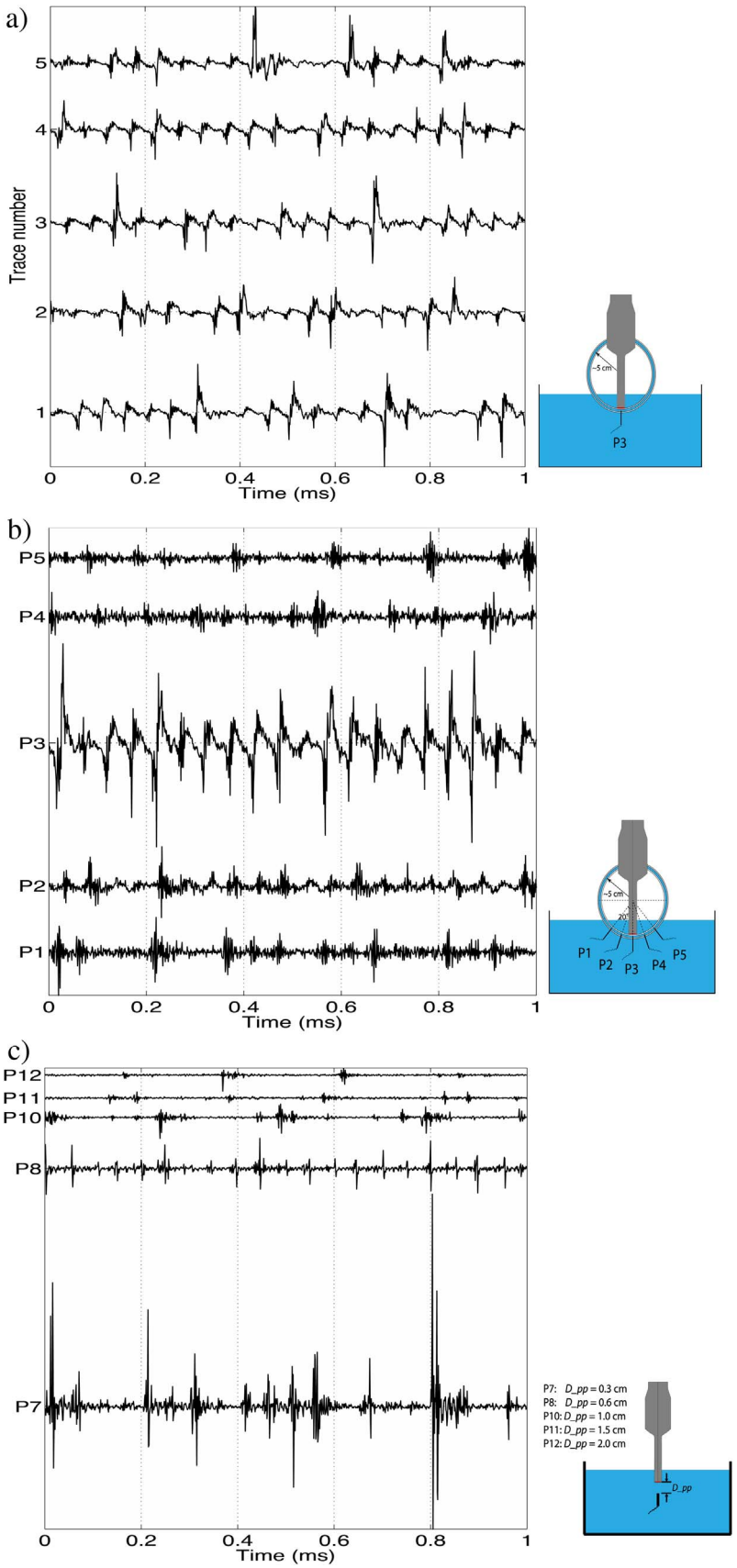

Fig. 2. Representative traces (i.e., time profiles of pressure voltage) measured by the pinducer at the measurement locations in (a) Fig. 1a, (b) Fig. 1b, and (c) Fig. 1c. For convenience of viewing, all trace data are normalized based on the largest amplitude value in the same figure. For each measurement location, 82 traces with time duration of ~3.7 s per trace were measured and recorded. Experimental details are described in Subsection 2.1. For conciseness of presentation with enough detail for analysis, only the middle 1 millisecond for representative traces is shown. For example, Fig. 2a shows 5 traces for the same measurement location P3 (Fig. 1ab), and Figs. 2bc show 1 representative trace for each other measurement location.

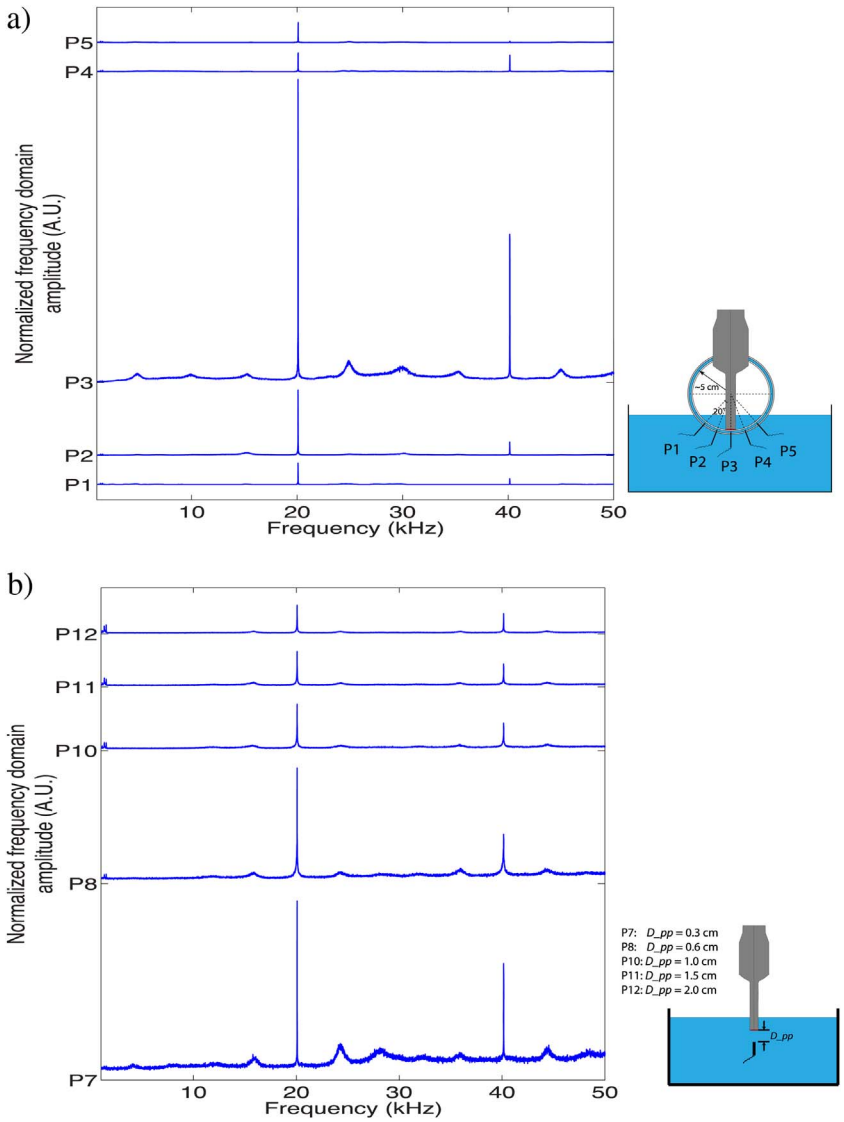

Fig. 3. Normalized frequency domain amplitudes ($A[k]$ in (3) and (4), indicating sonication intensity) for measurement points in (a) Fig. 1b and (b) Fig. 1c. For each measurement point, the highest amplitude peak height (intensity) is at 20 kHz, the ultrasound fundamental frequency (source frequency), as expected. Different amplitude peak positions and heights for different measurement points are analyzed in Section 3.1. The amplitudes for each measurement point are averaged for all 82 traces of full time duration, and normalized with respect to the amplitude at 20 kHz for P3 for (a) and P7 for (b), respectively. The frequency amplitudes at P3 and P7 are plotted together in Fig. 6c.

≥99%, from Sigma-Aldrich) was used as the solute and deionized water as solvent, which was pumped by a peristaltic pump (model Masterflex pump drive 7521-40, Easy Load II pump head with model no. 77200-50) at a mass flow rate of ~ 4 g/min through the tube. A temperature-controlled water bath (Fig. 5) removed heat generated from continuous ultrasonication and maintained a constant temperature at the nucleation zone.

2.3. Methods for pinducer data analysis

In theory, the acoustic intensity (unit: W/m^2) for a continuous time-series acoustic pressure trace $a(t)$ (unit: voltage) can be calculated as [29,30]

$$AI = \frac{1}{\rho c \tau}\int_0^{\tau} |p(t)|^2 dt = \frac{1}{\rho c \tau S^2}\int_0^{\tau} |a(t)|^2 dt \quad (1)$$

where AI denotes the total acoustic intensity for one trace (termed "total intensity" in this paper), $p(t)$ (unit: Pa) denotes the real acoustic pressure trace, ρ and c denotes the density and the sound velocity of the media where the acoustic wave propagate, τ denotes the total time of the trace, and S is the conversion factor between pressure $p(t)$ and pinducer measurement voltage $a(t)$. All four parameters (ρ = 1000 kg/m^3, c = 1500 m/s, τ = 0.1 s, S is considered an unknown constant) will not affect the normalized acoustic intensity such as in Fig. 4 and Table 1, as long as their values remain constant.

In real experimental systems (such as in this article), a discrete-time signal $a[n]$ of length N is usually measured instead of a continuous $a(t)$. The integration in (1) is approximated as

$$AI = \frac{1}{\rho c \tau S^2}\int_0^{\tau} |a(t)|^2 dt \approx \frac{1}{\rho c \tau S^2}\left(\sum_{n=0}^{N-1} |a[n]|^2\right) \quad (2)$$

where N is the length of $a[n]$ (N = 100,000 here for the number of data points within each trace time).

Parseval's Theorem allows the conversion between the time domain and frequency domain through the concept of signal energy (*Energy*) in [30]

$$Energy = \sum_{n=0}^{N-1} |a[n]|^2 = \frac{1}{N}\sum_{k=0}^{N-1} |A[k]|^2 \quad (3)$$

where k = 0, 1, …,N denotes the index in the frequency domain and

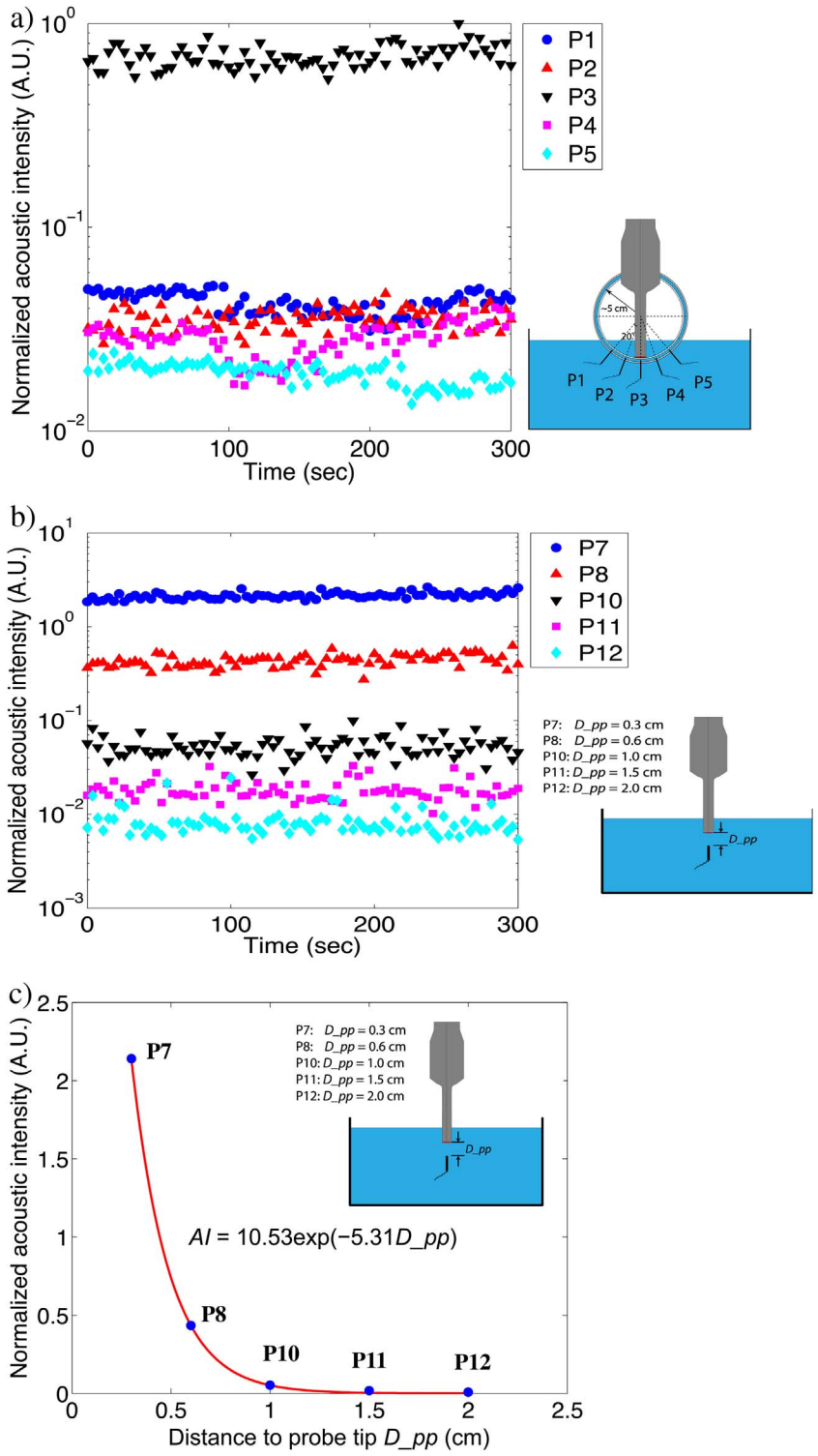

Fig. 4. Time profiles of normalized total acoustic intensity for various measurement locations in (a) Fig. 1b and (b) Fig. 1c. The intensity values are calculated using (2), normalized with respect to the maximum P3 value (e.g., as shown in (a)), with statistics listed in Table 1. (c) Plot of the mean total ultrasound intensity (values reported in Table 1) at different distances between pinducer tip to ultrasonic probe tip without using a tube (or "below the probe tip," with configurations in Fig. 1c). The distance between probe tip and tube circle center on probe (the reference point "distance" in Table 1) is ~4.7 cm.

$n = 1,2,\ldots,N$ denotes the index in the time domain. Comparing (2) and (3), the signal energy can be approximated by the total intensity through multiplying by a constant. The term $\frac{1}{N}|A[k]|^2$ corresponds to the signal energy (and total intensity) at the kth frequency. The domain conversion from time to frequency is achieved through discrete Fourier transform of $a[n]$ [31]:

$$A[k] = \sum_{n=0}^{N-1} a[n] e^{-2\pi i k n/N} \tag{4}$$

3. Results and discussion

Pinducer measurements (Fig. 2), together with quantitative analysis

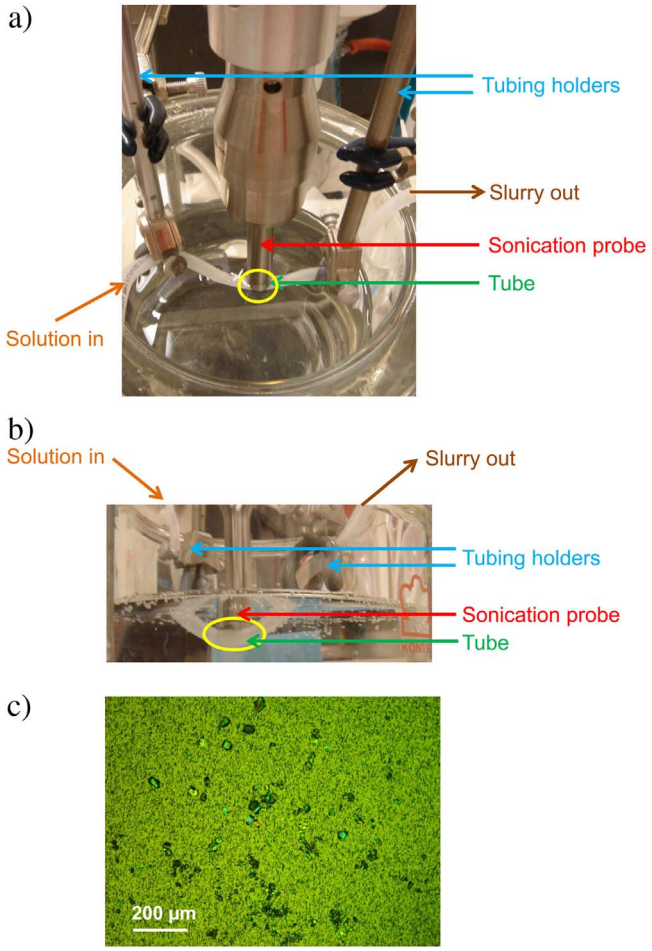

Fig. 5. Photograph of the ultrasonication setup for nucleation validation at (a) an upper view and (b) a side view. Nucleation experimental details are described in Subsection 2.2, with the design justification and optimization in Subsection 3.2. The focused indirect sonication zone is highlighted in yellow, based on the pinducer learnings for closely around the P3 point in Fig. 1b. (c) Microscope (with polarizers) images of nuclei generated by cooling nucleation in the ultrasonication setup shown in (a) and (b). The tiny black dots on the background are the pores (pore diameter of 2 μm) of the membrane filter where the slurry containing the nuclei was filtered. No images are provided for the same setup without using ultrasonication, as there is barely any nuclei on top of the membrane filter in most views (also confirmed by Ref. [5] at the same nucleation condition).

for frequency (Fig. 3) and total intensity (Fig. 4), were used to evaluate different configurations of ultrasonic configurations, and to design and optimize the ultrasonication-aided nucleation setup (Fig. 5).

3.1. Signal analysis for different ultrasonic configurations

The time profiles of amplitudes (vertical axis in Fig. 2, proportional to pressure) provide quick qualitative information of the system. For example, the time-variant amplitudes and shapes between different traces in Fig. 2a suggest that, during continuous ultrasonication, the pressure can vary at the same physical location even within the time scale of milliseconds. The measurement at P3 (Fig. 2a, with configuration in Fig. 1a) has higher amplitude in general than other physical locations with the same tubing such as P2 and P4 (Fig. 2b), indicating that pressure is not spatially uniform. The spatial and time non-uniformity of pressure can be explained by the combined effect of pressure field and the complex interaction with its consequent phenomena such as cavitation. For most traces collected at P3 of energy transferred through tubing (e.g., Fig. 2a), the general period of amplitude is roughly 0.05 ms, indicating a frequency of 20 kHz. The periodicity is not as strong for traces at other measurement locations (e.g., Fig. 2bc).

Table 1
Statistics of total intensities at different pinducer measurement points (Fig. 1)[a].

Photograph and analysis	Angle; distance (cm)	Mean, total intensity (a.u.)	Standard error, total intensity (a.u.)	Coefficient of variation, total intensity
P1 in Fig. 1b	40°; 5	0.0427	0.00059	0.13
P2 in Fig. 1b	20°; 5	0.0352	0.00047	0.12
P3 in Fig. 1b	0°; 5	0.6910	0.00967	0.13
P4 in Fig. 1b	20°; 5	0.0283	0.00059	0.19
P5 in Fig. 1b	40°; 5	0.0192	0.00025	0.12
P7 in Fig. 1c	0°; 5.0 (D_pp = 0.3)	2.1414	0.01904	0.08
P8 in Fig. 1c	0°; 5.3 (D_pp = 0.6)	0.4345	0.00720	0.15
P10 in Fig. 1c	0°; 5.7 (D_pp = 1.0)	0.0534	0.00149	0.25
P11 in Fig. 1c	0°; 6.2 (D_pp = 1.5)	0.0183	0.00050	0.25
P12 in Fig. 1c	0°; 6.7 (D_pp = 2.0)	0.0084	0.00034	0.37

[a] Each measurement location refers to a specific pinducer placement. Measurement locations P1–P5 in Fig. 1b have tubing, while P7–P12 in Fig. 1c do not. (As seen from the numbering for the measurement locations, only representative locations and data are shown here to convey the knowledge and message within limited space without confusion; while other measurement locations following the same trend such as P6 and P9 not shown here serve as confirmation of the analysis.) "Angle" refers to the angle between the longitudinal direction of the ultrasonic probe and the pinducer as shown in Fig. 1b for nonzero angles, and Fig. 1c for zero angles. "Distance" refers to the distance along the longitudinal direction of pinducer between pinducer tip and the tubing ring center (on the ultrasonic probe as shown in Fig. 1b). The values of D_pp for Fig. 1c are also included. Detailed description for equipment set up is in Subsection 2.1 and in Figs. 1abc. The total intensities for every trace of each experiment (each measurement point in Fig. 1bc), where the statistics (mean, standard error, and coefficient of variation) are based on, were calculated using (2) after normalization with respect to the maximum total intensity value at P3 (the same as in figures on total intensities such as Fig. 4 for convenient comparison).

The periodicity is quantified with frequency analysis using the discrete Fourier Transform, such as the magnitude of the highest peak in all spectra in Fig. 3 (corresponding to all measurement locations for Fig. 2), which is at the ultrasound source frequency (or fundamental frequency, f = 20 kHz) and mainly from the ultrasound source and cavitations [26]. The existence of the fundamental frequency peak confirms the sonic effect in water medium (Figs. 3 and S1b) but not in air medium (P0.1 and P5.9 in Fig. S1b, P7a in Fig. 6c), which can be explained by a much larger value of acoustic impedance for water than air [29]. Other frequency peaks are due to bubble oscillations and complex interactions (e.g., between multiple bubbles, tubing, probe, and pinducer). For example, subharmonics (f/n, n = 2, 3, 4, …) are explained as being from "active cavitation" bubbles (high-energy collapse followed by fragmentation and generation of new cavitation nuclei, as defined in [16]), harmonics (mf, m = 2, 3, 4, …) from forced nonlinear bubble oscillations, and the noise background from shock waves emitted by the collapsing bubbles, as summarized in Ref. [26]. Although the ultrasound fundamental frequency is at 20 kHz, the consequence can be a wide range of frequency (Figs. 3ab, 6c, and S1b). This discovery of a wide frequency distribution can provide more insight for the continuous ultrasonication-aided physicochemical phenomena such as crystallization [1,4,5,8–13,15,17,19–21]. An immediate example would be to analyze the effective frequency for a system, so as to understand and correlate the fundamental frequency and sonication parameters to the nuclei or crystal size distribution.

The total acoustic intensity can be quantified based on the pressure amplitudes using (2). The time-variant total intensities in Fig. 4ab for each configuration are indicated by the shape and amplitude variations of pressure time profiles (traces) in Fig. 2, and the frequency amplitudes in Fig. 3. Higher pressure amplitudes contribute to higher energy intensity of the system. The P3 region, which has the highest amplitude

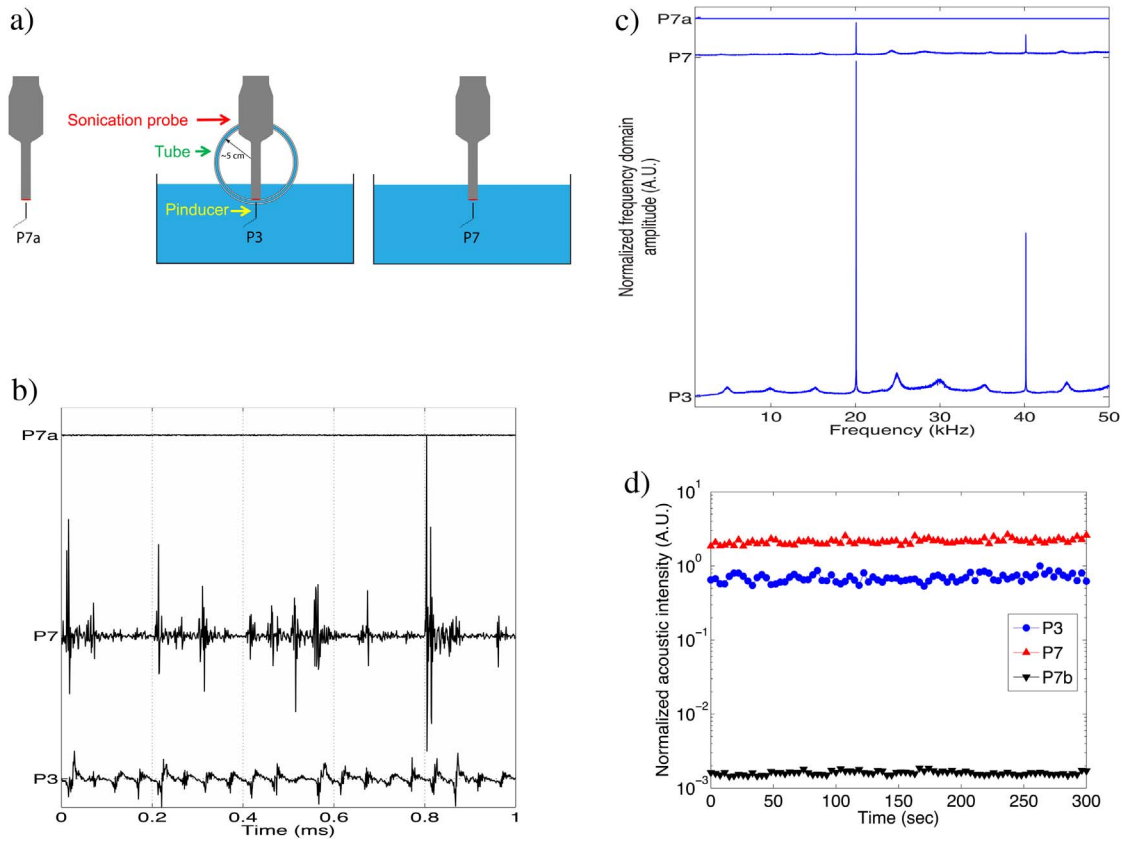

Fig. 6. (a) Diagram of the same pinducer placement in different media (P7a with air, P3 with tubing and water as in Fig. 1b, and P7 with water as in Fig. 1c, respectively). (b) Representative traces for pinducer measurements in (a), with amplitudes normalized with respect to the largest value in the same figure for convenient viewing. (c) Normalized frequency domain amplitudes, averaged for all traces of P3, P7, and P7a in (a), normalized with respect to the amplitude at 20 kHz for P3 in Fig. 3a. (d) The time profile of the total acoustic intensity for pinducer measurements in (a), normalized with respect to the maximum total intensity at P3 (e.g., as shown in Fig. 4a).

in Fig. 2b, receives the highest intensity among the five configurations (P1–P5, Fig. 1b), as shown in the mean total intensities in Table 1, and the total intensity profiles in Fig. 4a. The comparison shows that the ultrasound intensity inside the tubing is highest directly under the ultrasonic probe (P3 in Fig. 1b), compared to nonzero angles along the tubing (e.g., P1, P2, P4, P5, in Figs. 3a and 4a, and Table 1), even as small as a 20° (~ 2 cm downstream or upstream). The total intensity is even smaller when tubing was near air/water interface or in air medium further downstream (see P0.1, P0.5, P5.5, and P5.9 in Figs. 1b and S1). The much higher intensity at P3 compared to other locations inside the tube indicates a localized (aka "focused") effective sonication zone (P3) for nucleation. For ultrasonication without use of the tube, the coefficients of variation in the sonication intensity are significantly higher (i.e., ≥0.25) beyond 1 cm of the center of the ultrasonic probe tip (Table 1 and Fig. 1c). For indirect focused ultrasonication within the tube, the coefficients of variation remain small (e.g., ≤0.2) for a farther distance from the probe tip (Table 1 and Fig. 1b). For example, the coefficients of variation for low for P1 and P5 are $2\pi(5\text{ cm})(40^\circ)/180^\circ = 7$ cm away from the center of the probe tip, which are the farthest points measured in the tube.

Along the longitudinal direction of the ultrasonic probe, the ultrasound/cavitation intensity is higher with smaller distance (without contacting the probe tip) between ultrasonic probe tip and measurement point (e.g., Figs. 3b and 4bc), which agrees with physical intuition and relevant studies that energy dissipation increases with a longer distance [6,14,18,32]. The experimental results in Fig. 4c show that the measured intensity decays exponentially as a function of distance, dropping by more than two orders-of-magnitude for each 1 cm increase in distance. The distance dependence of the ultrasound intensity can facilitate the design of ultrasound-aided crystallizers of various configurations (e.g., Refs. [10,12,17]), by identification of the spatial zone with desired intensity and its spatial distribution for crystal distribution data analysis.

3.2. Nucleation validation and design analysis/optimization

Based on the above learnings, mainly the generation of a focused indirect sonication zone within a tube, a simple but effective nucleation setup was designed (Fig. 5ab). The focused localized ultrasonication zone is right under the ultrasonic probe, about the middle third of the length of tubing under water (as highlighted in yellow in Fig. 5ab), taking 1 s for the solution to flow through. Justifications for the experimental design are:

(1) The tube outer diameter (~6 mm) is chosen to be smaller than the tip diameter of the sonication probe (~10 mm), to ensure that all of the fluid within the tube right under the probe is under high-intensity sonication. These dimensions are selected because the sonication intensity sharply drops with distance from the probe centerline (e.g., comparing the P3 location with P4 or elsewhere).
(2) The tube material is chosen to be pliant but resistant to cavitation-induced damage, to minimize mechanical breakage when in direct physical contact with the sonication probe, and should have a surface that is resistant to the sticking of crystals. A tube made of silicone meets these criteria, although other tubing materials that satisfy these properties would be viable alternatives.
(3) The fluid outside the tube, water, is selected to have a high thermal diffusivity so that heat generated during sonication is conducted away from the region of high-intensity sonication, to limit the increase in local temperature. Any fluid with high thermal diffusivity could be used in place of water.
(4) The probe tip is pressed tightly against the tubing wall to minimize

the distance between the fluid in the tubing and the probe tip (Fig. 5a) to maximize acoustic energy intensity; and

(5) Higher intensity is achieved by using water as the medium instead of air through the gap between the flat ultrasonic probe tip and the curved outer surface of the tubing, as indicated by the higher total intensity of P7 than P7a of the same distance with different media in Fig. 6d.

Nuclei of improved size uniformity and reduced aggregation were generated (Fig. 5c) for a solute that tends to aggregate [5,24]. The solution has a narrow residence time distribution under effective sonication past the small focused region, when the solution flow rate remains constant. The small size of the region reduces the effect of spatial heterogeneity of ultrasound intensity for nucleation, compared to placing a probe in the container or a long tube in the bath where a much larger volume is exposed to ultrasonication [26]. The improved spatial uniformity of ultrasonication (thus the nuclei generation) increased the reproducibility and scalability of the process (e.g., through running the continuous flow and ultrasonication for a longer time using the same equipment, within the equipment operation limit).

The identification of the small ultrasonic region also allows further optimization of existing nucleation designs to control nuclei size distribution: (1) the distance from probe to tubing (sample) provides an additional degree of freedom for manipulating intensity inside tubing, and ultrasonic amplitude, which had been shown effective [5]; and (2) the distance can be greatly reduced between the ultrasonication region (the “nucleation zone” in [5]) and downstream subprocesses (e.g., [5] left 70 cm for a safe distance before the inlet of compressible gas), as indicated from the fast decay of intensity downstream of P3 (Fig. 4a). The reduction in this distance would narrow the residence time distribution.

4. Conclusions

A pinducer was applied for high-speed measurement of pressure to guide the design of a setup for nucleating crystals inside a tube under ultrasonication. The pinducer measurement quantifies the transfer of ultrasonic energy through the tubing wall to fluid inside the tube, and identifies the localized zone for nucleation right under the probe. The higher the distance from the ultrasonic probe tip along the longitudinal dimension, the lower the intensity. The fluctuations in pressure intensity suggest that nucleation rates induced by ultrasonication, even in such a localized and “protected” environment, will exhibit some fluctuations. Discrete Fourier Transform analysis also indicated that, in addition to 20 kHz (ultrasonic source) being a key frequency for the energy transferred to fluid inside tubing, complex interactions (e.g., multiple bubbles, tubing) are observed by other frequencies (e.g., harmonics) within the system, which can all contribute to a secondary effect such as nucleation.

These analyses suggest some interesting research questions that include: (1) What are the fundamental physics behind the differences in intensities between P3 and P7 at the same distance from the probe tip: P3 with tubing has a much higher amplitude (thus intensity) at 20 kHz (the fundamental frequency) compared to P7 without tubing (Fig. 6c), although the total intensity for P3 is much smaller (Fig. 6d). (2) Can the effective frequency distribution be quantitatively correlated to the nuclei or crystal size distribution? Based on the pinducer learnings, nucleation using focused indirect ultrasonication was set up, with technical details analyzed and further improvement suggested for optimization of existing probe-based designs. Using Ref. [5] as an example, the tubing is suggested to be placed as close to the ultrasonic probe tip as possible, with reasonably short length downstream before slug formation, for efficient stable ultrasonic energy intensity and narrower residence time distribution inside tubing. The high-speed measurement of spatially heterogeneous ultrasound intensity can be applied to other crystal systems as well. For example, the spatial distribution of energy intensities would also be relevant for the design of ultrasonication-based crystal breakage, which is a process for converting needle-like crystals to crystals of lower aspect ratios [1].

Acknowledgements

Novartis Pharmaceuticals is acknowledged for financial support. Prof. M. Nafi Toksöz, Dr. Zhenya Zhu, and Dr. Jun Xu at MIT are thanked for pinducer measurement equipment setup and operation, and helpful technical discussion.

Appendix A. Supplementary data

Supplementary data associated with this article can be found, in the online version, at http://dx.doi.org/10.1016/j.cep.2017.04.008.

References

[1] J.R.G. Sander, B.W. Zeiger, K.S. Suslick, Sonocrystallization and sonofragmentation, Ultrason. Sonochem. 21 (2014) 1908–1915, http://dx.doi.org/10.1016/j.ultsonch.2014.02.005.
[2] H. Li, J. Wang, Y. Bao, Z. Guo, M. Zhang, Rapid sonocrystallization in the salting-out process, J. Cryst. Growth 247 (2003) 192–198, http://dx.doi.org/10.1016/S0022-0248(02)01941-3.
[3] N. Amara, B. Ratsimba, A.M. Wilhelm, H. Delmas, Crystallization of potash alum: effect of power ultrasound, Ultrason. Sonochem. 8 (2001) 265–270, http://dx.doi.org/10.1016/S1350-4177(01)00087-6.
[4] M.D. Luque de Castro, F. Priego-Capote, Ultrasound-assisted crystallization (sonocrystallization), Ultrason. Sonochem. 14 (2007) 717–724, http://dx.doi.org/10.1016/j.ultsonch.2006.12.004.
[5] M. Jiang, C.D. Papageorgiou, J. Waetzig, A. Hardy, M. Langston, R.D. Braatz, Indirect ultrasonication in continuous slug-flow crystallization, Cryst. Growth Des. 15 (2015) 2486–2492, http://dx.doi.org/10.1021/acs.cgd.5b00263.
[6] T. Terahara, S. Mitragotri, J. Kost, R. Langer, Dependence of low-frequency sonophoresis on ultrasound parameters; distance of the horn and intensity, Int. J. Pharm. 235 (2002) 35–42, http://dx.doi.org/10.1016/S0378-5173(01)00981-4.
[7] T.J. Mason, J.P. Lorimer, Applied Sonochemistry: The Uses of Power Ultrasound in Chemistry and Processing, Wiley-VCH Verlag, GmbH, Weinheim, 2002.
[8] S. Gracin, M. Uusi-Penttilä, Å.C. Rasmuson, Influence of ultrasound on the nucleation of polymorphs of p-aminobenzoic acid, Cryst. Growth Des. 5 (2005) 1787–1794, http://dx.doi.org/10.1021/cg050056a.
[9] G. Ruecroft, D. Hipkiss, T. Ly, N. Maxted, P.W. Cains, Sonocrystallization: the use of ultrasound for improved industrial crystallization, Org. Process Res. Dev. 9 (2005) 923–932, http://dx.doi.org/10.1021/op050109x.
[10] H.N. Kim, J.R.G. Sander, B.W. Zeiger, K.S. Suslick, Spray sonocrystallization, Cryst. Growth Des. 15 (2015) 1564–1567, http://dx.doi.org/10.1021/acs.cgd.5b00072.
[11] S. Devarakonda, J.M.B. Evans, A.S. Myerson, Impact of ultrasonic energy on the flow crystallization of dextrose monohydrate, Cryst. Growth Des. 4 (2004) 687–690, http://dx.doi.org/10.1021/cg034173m.
[12] S.V. Dalvi, R.N. Dave, Controlling particle size of a poorly water-soluble drug using ultrasound and stabilizers in antisolvent precipitation, Ind. Eng. Chem. Res. 48 (2009) 7581–7593, http://dx.doi.org/10.1021/ie900248f.
[13] O. Narducci, A.G. Jones, E. Kougoulos, Continuous crystallization of adipic acid with ultrasound, Chem. Eng. Sci. 66 (2011) 1069–1076, http://dx.doi.org/10.1016/j.ces.2010.12.008.
[14] V.S. Sutkar, P.R. Gogate, Design aspects of sonochemical reactors: techniques for understanding cavitational activity distribution and effect of operating parameters, Chem. Eng. J. 155 (2009) 26–36, http://dx.doi.org/10.1016/j.cej.2009.07.021.
[15] A. Soare, R. Dijkink, M.R. Pascual, C. Sun, P.W. Cains, D. Lohse, A.I. Stankiewicz, H.J.M. Kramer, Crystal nucleation by laser-induced cavitation, Cryst. Growth Des. 11 (2011) 2311–2316, http://dx.doi.org/10.1021/cg2000014.
[16] M. Ashokkumar, The characterization of acoustic cavitation bubbles – An overview, Ultrason. Sonochem. 18 (2011) 864–872, http://dx.doi.org/10.1016/j.ultsonch.2010.11.016.
[17] R.J.P. Eder, S. Schrank, M.O. Besenhard, E. Roblegg, H. Gruber-Woelfler, J.G. Khinast, Continuous sonocrystallization of acetylsalicylic acid (ASA): Control of crystal size, Cryst. Growth Des. 12 (2012) 4733–4738, http://dx.doi.org/10.1021/cg201567y.
[18] D. Rossi, R. Jamshidi, N. Saffari, S. Kuhn, A. Gavriilidis, L. Mazzei, Continuous-flow sonocrystallization in droplet-based microfluidics, Cryst. Growth Des. 15 (2015) 5519–5529, http://dx.doi.org/10.1021/acs.cgd.5b01153.
[19] A. Kordylla, S. Koch, F. Tumakaka, G. Schembecker, Towards an optimized crystallization with ultrasound: effect of solvent properties and ultrasonic process parameters, J. Cryst. Growth. 310 (2008) 4177–4184, http://dx.doi.org/10.1016/j.jcrysgro.2008.06.057.
[20] H. Siddique, C.J. Brown, I. Houson, A.J. Florence, Establishment of a continuous sonocrystallization process for lactose in an oscillatory baffled crystallizer, Org. Process Res. Dev. 19 (2015) 1871–1881, http://dx.doi.org/10.1021/acs.oprd.5b00127.
[21] S. Kim, C. Wei, S. Kiang, Crystallization process development of an active

pharmaceutical ingredient and particle engineering via the use of ultrasonics and temperature cycling, Org. Process Res. Dev. 7 (2003) 997–1001, http://dx.doi.org/10.1021/op034107t.
[22] H.M. Santos, J.L. Capelo, Trends in ultrasonic-based equipment for analytical sample treatment, Talanta 73 (2007) 795–802, http://dx.doi.org/10.1016/j.talanta.2007.05.039.
[23] S. Kudo, H. Takiyama, Production of fine organic crystalline particles by using milli segmented flow crystallizer, J. Chem. Eng. Japan 45 (2012) 305–309, http://dx.doi.org/10.1252/jcej.11we168.
[24] M. Jiang, Y.-E. Li, H.-H. Tung, R.D. Braatz, Effect of jet velocity on crystal size distribution from antisolvent and cooling crystallizations in a dual impinging jet mixer, Chem. Eng. Process. 97 (2015) 242–247, http://dx.doi.org/10.1016/j.cep.2015.09.005.
[25] R. Lakerveld, N.G. Verzijden, H. Kramer, P. Jansens, J. Grievink, Application of ultrasound for start-up of evaporative batch crystallization of ammonium sulfate in a 75-L crystallizer, AIChE J. 57 (2011) 3367–3377, http://dx.doi.org/10.1002/aic.12553.
[26] V.S. Moholkar, S.P. Sable, A.B. Pandit, Mapping the cavitation intensity in an ultrasonic bath using the acoustic emission, AIChE J. 46 (2000) 684–694, http://dx.doi.org/10.1002/aic.690460404.
[27] Z. Zhu, X. Liu, C. Gu, M.N. Toksöz, Experimental studies of the acoustic wavefield near a borehole, SEG Tech. Progr. Expand. Abstr. (2013) 514–518.
[28] P. Mougin, D. Wilkinson, K.J. Roberts, In situ measurement of particle size during the crystallization of l-glutamic acid under two polymorphic forms: influence of crystal habit on ultrasonic attenuation measurements, Cryst. Growth Des. 2 (2002) 227–234, http://dx.doi.org/10.1021/cg0155752.
[29] P.M. Morse, K.U. Ingard, Theoretical Acoustics, Princeton University Press, Princeton, N.J, 1986.
[30] A.V. Oppenheim, A.S. Willsky, S.H. Nawab, Signals and Systems, 2nd ed., Prentice Hall, Upper Saddle River, New Jersey, 1997.
[31] K.E. Atkinson, An Introduction to Numerical Analysis, 2nd ed., Wiley, New York, 1989.
[32] J. Klíma, A. Frias-Ferrer, J. González-García, J. Ludvík, V. Sáez, J. Iniesta, Optimisation of 20 kHz sonoreactor geometry on the basis of numerical simulation of local ultrasonic intensity and qualitative comparison with experimental results, Ultrason. Sonochem. 14 (2007) 19–28, http://dx.doi.org/10.1016/j.ultsonch.2006.01.001.